Indian Journal of Pure & Applied Physics
Vol. 55, September 2017, pp. 625-629

Determination of defect density, crystallite size and number of graphene layers in graphene analogues using X-ray diffraction and Raman spectroscopy

Rahul Sharma, Neakanshika Chadha & Parveen Saini*

Conjugated Polymers & Graphene Technology Laboratory, CSIR-National Physical Laboratory, New Delhi 110 012, India

Received 4 January 2017; accepted 14 May 2017

In this study, X-ray diffraction and Raman spectroscopic techniques have been wielded for determination of number of graphene layers per domain, crystallite size, interlayer spacing and defect density in bulk samples of chemically synthesized graphitic oxide (GrO) and reduced GrO (RGrO). Particularly, the ready to use and general mathematical equations have been presented for obtaining above mentioned parameters directly using the full width half maxima (FWHM) of XRD peaks and intensity ratios of Raman D- and G-bands. The results reflect that upon reduction, crystallites shrink in dimensions ultimately leads to decrease in number of graphene layers per domain and apparent increase in defect density.

Keywords: Graphitic oxide, Graphene, Reduced graphitic oxide, Raman Spectroscopy, D-band, G-band, Defect density, Crystallite size, sp^2 domains, X-ray diffraction, Full width half maximum

1 Introduction

Graphene, an atomically-thick 2D-hexagonal array of sp^2 hybridised carbon atoms, is the strongest, stiffest and thinnest material ever known, with ultra-large specific surface area along with excellent electrical and thermal properties[1–6]. Consequently, graphene based composites, coated substrates, 2D film materials and 3D assembled monolithic materials, are extensively explored and their tremendous potential in numerous applications such as energy storage, environmental remediation, EMI shielding, static charge mitigation, sensors and biomedicals[4–13], has been demonstrated. However, the expected properties and performance in practical applications of these materials are solely governed by the quality of constituent graphene phase and its assembled organization. Lately, the graphitic become the standard graphene precursors[4,10,13–15] and assurance of their quality in graphene analogues based macroscopic forms, viz; powders, flakes membranes, papers, coatings, foams, aerogels and composites, etc., is of prime importance[5]. In particular, the parameters like defect density, number of graphene layers, crystallite sizes of graphitic domains and presence of functional groups/dopant atoms, are known to play decisive role in the quality determination of graphene based materials. It is worth mentioning here that the structure of GrO and RGrO is generally probed by specific characterization tools including transmission electron microscopy (TEM), high resolution TEM (HRTEM), scanning electron microscopy (SEM), atomic force microscopy (AFM), raman spectroscopy and X-ray diffraction[4,16–18] (XRD). However, the HRTEM and AFM are limited to characterize ultra-thin samples possessing single-layer or few-stacked-layers of graphene analogues, whereas SEM provides only surface information and that too with a limited resolution. Further, they include specialized and tedious methods to prepare analytes, which often inadvertently disturbs the sample morphology and tends to give information of unintentionally tempered sample. Moreover, these techniques can not accurately predict the domain thickness, sp^2 domain sizes and [illegible]s, they are extremely sensitive toward surface cleanliness (SEM/AFM) and presence of foreign particles/impurities (TEM/HRTEM). Therefore, the information obtained by these characterisation tools cannot be extrapolated to predict the properties of bulk samples or macroscopic forms. In such conditions, the well-known diffraction and spectroscopic techniques such as XRD and Raman spectroscopy, respectively, comes to the rescue, and are considered highly advantageous for characterization of bulk quantity and macroscopic forms of graphene analogues[19]. Here, we have demonstrated a simple and effective methodology for

*Corresponding author (E-mail: pksaini@nplindia.org)

quality assessment of GrO and RGrO structures in terms of number of graphene layers, defect states, crystallite sizes and extent of conjugation, using XRD technique in conjunction with Raman microscopy. The various mathematical equations and related assumptions have been described and the evaluated parameters have been tabulated, compared and discussed for establishing the correlation between structural characteristics of GrO and RGrO phases and their XRD peaks and Raman bands.

2 Experimental Details

2.1 Materials

Graphite powder (CDH, India), sulphuric acid (98% Merck, India), sodium nitrate (Fisher Scientific, India), potassium permanganate (Fisher Scientific, India), hydrogen peroxide (Speck Pure chemicals, India), hydrochloric acid (37%, MERCK, India), hydrazine hydrate (Thomas Baker, India) were of analytical grade and used on as received basis. Distilled water having resistivity >10^6 ohm-cm was used for synthesis and washing.

2.2 Synthesis of GrO and RGrO

GrO was prepared by modified hummers method[5,20] using powdered graphite as precursor. In a typical synthesis, 3 g powdered graphite was added to the mixture of sulphuric acid (70 mL, 98%) and sodium nitrate (3 g), and contents were stirred magnetically. After 1 h, 9 g of potassium permanganate was added very slowly to the reaction mixture kept at ice bath thereby keeping temperature below 20 °C so as to control exothermicity of the reaction. Subsequently, the reaction mixture was kept for stirring at room temperature. Intense brown colour fumes were released during the initial phase of potassium permanganate reaction with graphite mixture. After 18 h of stirring, a purple coloured paste was formed which upon dilution with distilled water changed to brown with brisk effervescences accompanied by enhancement of reaction mixture temperature to 98 °C. After 20 min of stirring, the brown colour mixture was further diluted with distilled water followed by addition of hydrogen peroxide, leading to colour change of mixture to bright yellow. The yellow colour product was filtered-off and washed several times with dilute hydrochloric acid followed by warm water washing to remove the salts and acidic impurities. The neutral brown product then dried at 60 °C in vacuum oven to get the graphitic oxide (GrO) flakes. These flakes were dispersed in water, followed by solvent casting to obtain GrO based paper like material. A piece of GrO is exposed to hydrazine vapours at room temperature for 12 h, resulting in transformation of GrO phase to reduced graphitic oxide (RGrO).

2.3 Characterization

The X-ray diffraction (XRD) spectroscopic patterns of GrO and RGrO were recorded using Bruker D8 Advance X-ray diffractometer at a scan rate of 0.02°/s, slit width of 0.1 mm using CuKα line (λ= 1.540598 Å) as radiation source. Raman microscope (Renishaw In Via) was used for recording spectra with 514.5 nm laser as excitation source.

3 Results and Discussion

Figure 1(a) and (b) shows the XRD patterns of GrO and RGrO. It can be seen that GrO displays a single diffraction peak centred at 2θ value of 11.07° corresponding to inter-layer-spacing of 7.98 Å calculated using the equation:

$$d = \frac{\lambda}{2\mathrm{si}} \quad \ldots (1)$$

where d is the inter-layer spacing, θ is half of corresponding diffraction angle and λ is the wavelength of X-ray source. The calculated d value for GrO is found to be more than double compared to

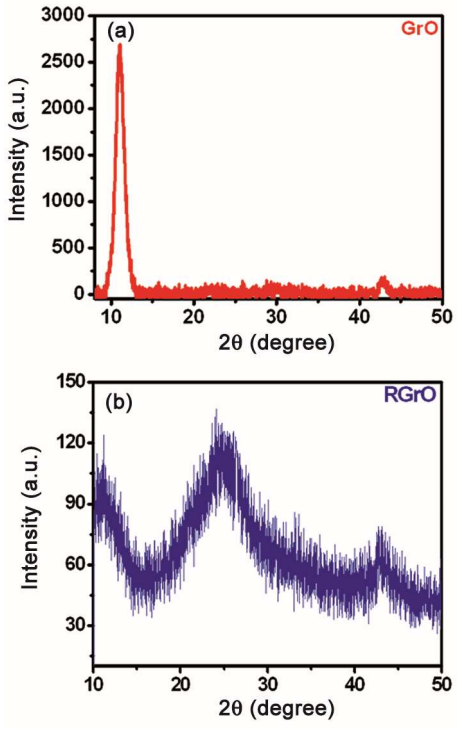

Fig. 1 — XRD patterns of (a) GrO and (b) RGrO

pristine graphite[5] (d~ 3.34 Å) which confirms the expansion of graphitic stack owing to formation of oxidation generated polar functionalities over graphene layers. It is noteworthy that due to hydrophilic nature of formed GrO, small amount of water molecules are always present as entrapped species between the layers, thus co-contributing toward observed d value. However, their contribution is very less compared to physical separation collectively caused by introduced functional groups as well as by sp^3 defects induced disturbance of planarity. Nevertheless, after reduction of GrO to RGrO, the peak shifted from ~11.07° to ~24.88° (Table 1), which confirms the reduction of inter-layer spacing to 3.57 Å for RGrO. This also reflects removal of oxygen rich functionalities and restoration of conjugation via regeneration of sp^2 domains.

In contrast to the XRD peak positions (that depends upon inter-layer spacing), the peak width is highly dependent on size of graphitic domains existing inside the macroscopic graphene materials. The domains are laterally separated by grain boundaries (the break in graphitic stacking) and longitudinally by sp^2/sp^3 domain boundaries. Particularly, the average crystallite width (D), i.e., the perpendicular dimension within which the graphitic ordering is maintained (shown schematically in Fig. 2(a)), is given by well-known Debye-Scherer equation[21]:

$$D = \frac{K\lambda}{\beta co} = \frac{0.89\lambda}{\beta \cos\theta} \quad \ldots (2)$$

where β is the full peak width of the diffraction peak at half maximum height (FWHM) expressed in radians (schematic Fig. 2(b)); θ is half diffraction angle of peak corresponding to inter-layer spacing (2θ ~ 11° for GrO and 2θ ~ 24° for RGrO); and K is a constant related to crystallite shape, normally taken as 0.89 for spherical crystals with cubic unit cells. Similarly, in-plane crystallite size (L) can be expressed in terms of in-plane periodicity peak (2θ ~43°) as:

$$L = \frac{1.84\lambda}{\beta co} \quad \ldots (3)$$

It has been found that the average crystallite size (Table 1) significantly decreases in RGrO (D ~ 8.2 Å; L ~ 258.0 Å) relative to GrO (D ~ 140.7 Å; L ~ 491.1 Å). This reflects the shrinking of graphitic domains (i.e., disruption of graphitic stacked ordering) and formation of more grain boundaries or lateral defects, which may occur due to expulsion of graphene layers from domains upon reduction. The average number of graphene layers (n) per domain can be calculated from XRD peak broadening using the combination of Debye-Scherrer and Bragg's equations (i.e. Eqs (1) and (2)) that gives the expression for n as:

$$n = \left(\frac{D}{d} + 1\right) = \left(\frac{2K\mathrm{ta}}{\beta} + 1\right) \quad \ldots (4)$$

The calculations show that there is significant reduction in graphene layer (n) per crystallite upon reduction, i.e., from n=17 for GrO to n=3 for RGrO. As the oxygen functionalities in GrO are responsible for strong molecular interaction (polar attractive forces) between individual layers and their consequent compact packing, the decrease in n upon reduction can be attributed to the elimination of functional groups and vanishing of inter-layer attractive interactions of GrO. The Raman spectra of GrO and RGrO have been shown in Fig. 3(a) and 3(b), respectively. It can be clearly seen that GrO gives two prominent Raman features at ~1355 cm^{-1} and ~1598 cm^{-1} corresponding to D and G bands, respectively. The G-peak corresponds to the first order scattering of the E_{2g} optical mode of sp^2 domains (i.e., due to in-plane vibrations of carbon atoms). In contrast, the D-peak is due to the disordered regions containing sp^3 carbons with associated out-of-plane vibrations.

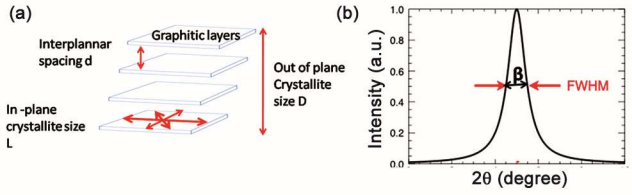

Fig. 2 — Schematic representation of (a) graphitic layers in crystallites, (b) FWHM of XRD peak

Table 1 — Various physical parameters of GrO and RGrO obtained from X-ray diffraction and Raman spectroscopy characterization technique

	XRD					Raman					
Parameters / Samples	2θ (degree)	D (Å)	D (Å)	Number of layers (n)	L (Å)	D-band (cm^{-1})	G-band (cm^{-1})	I_D/I_G ratio	L_{sp2} (nm)	L_D (nm)	$n_D \times 10^{11}$ (cm^{-2})
GrO	11.07	7.98	140.7	17	491.1	1355	1598	0.993	16.86	12.98	1.89
RGrO	24.88	3.57	8.2	3	258.0	1348	1596	1.155	14.50	12.04	2.196

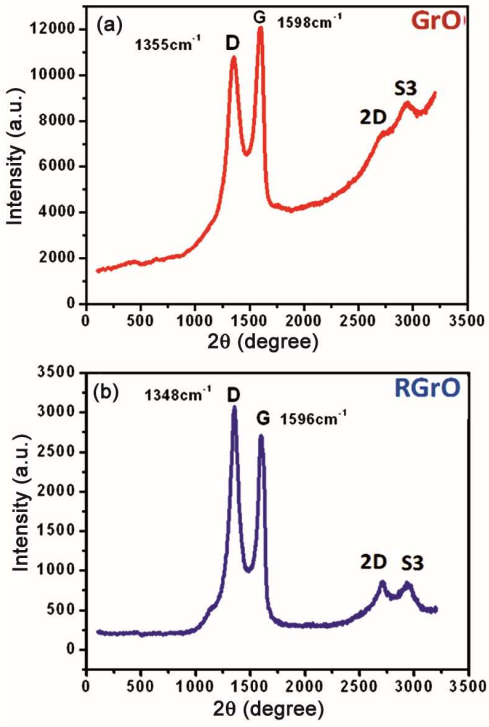

Fig. 3 — Raman spectra of (a) GrO and (b) RGrO

In addition to *G*- and *D*-bands, two weak peaks at ~2690 cm^{-1} (2*D*-band) and ~2930 cm^{-1} (*S*3-band) have also been observed in the Raman spectra of GO. The 2*D*-band is regarded as overtone of *D*-peak whereas *S*3 is attributed to the combination of *D* and *G* peaks (i.e., *G*+*D* band). In RGrO sample, the observed narrowing of *D*-band, broadening of *G*-band and the systematic variation of their position/intensity are indicative/signatures of reduction. Here, the reduction of GrO leads to systematic shifting of *D*, *G*, 2*D* and *S*3 peaks to about ~1348 cm^{-1}, ~1596 cm^{-1}, ~2709 cm^{-1} and~2945 cm^{-1}, respectively. The careful examination also shows that upon reduction, there is increase in relative intensity and decrease in width of 2*D* and *S*3 peaks, which reflects restoration of conjugation upon reduction. It is worth mentioning that the I_D/I_G ratio (i.e., integrated intensity ratio of raman *D*- and *G*-bands) is commonly exploited for estimation of in-plane size of sp^2 domains (L_{sp^2}), average defect distance (L_D) as well as defect density (n_D, cm^{-2}) using the following equations:

$$L_{sp^2} = \frac{560}{E_L^4}\frac{I_G}{I_D} \quad \ldots (5)$$

$$L_D^2(nm^2) = 2.4 \times 10^{-9}\lambda_L^4\frac{I_G}{I_D} \quad \ldots (6)$$

$$n_D = \frac{2.4\times10^{22}}{\lambda_L^4}\frac{I_D}{I_G} \quad \ldots (7)$$

where E_L and λ_L are the energy and wavelength of the Raman laser source, respectively. The Eqs (6) and (7) are valid for point like defects but not for edge defects, intercalants and charge impurities as the later ones do not change the intensity of *D*-band. The various values calculated from above discussed empirical equations and Raman spectra of GrO and RGrO are presented in Table 1. The observed I_D/I_G ratio (Table 1) and calculated across-plane and in-plane crystallite size (i.e., *D* and *L* values) trends revealed that in RGrO, more number of sp^2 domains are formed which are smaller in size compared to sp^2 domains of GrO. Such decrease in average size of sp^2 domains is in agreement with observed enhancement of I_D/I_G ratio upon reduction and consequent dwindling of the average defect size (L_D) in RGrO compared GrO. Accordingly, the calculated defect density (n_D) which is inversely related to the L_D, was also found to be inflated in RGrO (Table 1), suggesting the formation of more defects. As the reduction doesn't involve carbon-carbon bond cleavage, the reflected Sp^2 domains shrinkage is questionable, and require further systematic studies to resolve this mystery.

4 Conclusions

In this study, we have systematically presented some useful mathematical equations for the quantitative determination of in-plane and across-plane crystallite sizes, average number of graphene layers per domain, and defect density of graphene analogues. It was found that upon reduction, both the average number of graphene layers and average sp^2 crystallite size (*L*) decrease from 17 to 3 and 16.86 nm to 14.50 nm, respectively. In addition, an increase in defect density is observed after reduction, which along with increased I_D/I_G ratio reflects the increase in population of sp^2 domains at the expense of domain size.

Acknowledgement

The authors are grateful to Director, CSIR-National Physical laboratory, New Delhi, for providing necessary research facilities and constant encouragement for this work. RS and NC are thankful to UGC for providing award of Junior Research Fellowship. Authors are also thankful to Dr N Vijayan for XRD patterns. The work is partially supported by the DST-Young Scientist Fast Track Proposal (GAP141232) and the CSIR-Young Scientist Research Grant (OLP152832).

References

1 Geim A K & Novoselov K S, *Nat Mater*, 6 (2007) 183.
2 Lee C, Wei X, Kysar J W & Hone J, *Science*, 321 (2008) 385.
3 Chen J H, Jang C, Xiao S, Ishigami M & Fuhrer M S, *Nat Nanotechnol*, 3 (2008) 206.
4 Sharma R & Saini P, *Diamond and carbon composites and nanocomposites*, Eds Aliofkhazraei M A, (In-Tech publisher: Croatia), 2016.
5 Saini P, Kaushik S & Sharma R, *Eur Phys J B*, 89 (2016)1.
6 Saini P, Sharma R & Akodia S, *World J Text Eng Technol*, 2 (2016) 1.
7 Saini P, Kuila T, Saha S & Murmu N C, *Advanced sensor and detection materials*, Eds. Tiwari A & Demir M M, (Scrivener Publishing: Massachusetts, USA), (2014) 467.
8 Qiu L, Liu J Z, Chang S LY, Wu Y & Li D, *Nat Commun*, 3 (2012) 1241.
9 Zhou G, Paek E, Hwang G S & Manthiram A, *Nat Commun*, 6 (2015) 7760.
10 Yao H B, Ge J & Wang C F, *Adv Mater*, 25 (2013) 6692.
11 Sun H, Xu Z & Gao C, *Adv Mater*, 25 (2013) 2554.
12 Chen Z, Xu C, Ma C, Ren W & Cheng H M, *Adv Mater*, 25 (2013) 1296.
13 Bi H, Xie X & Yin K, *Adv Funct Mater*, 22 (2012) 4421.
14 Tripathi S N, Saini P, Gupta D & Choudhary V, *J Mater Sci*, 48 (2013) 6223.
15 Hu H, Zhao Z, Wan W, Gogotsi Y & Qiu J, *Adv Mater*, 25 (2013) 2219.
16 Moon I K, Lee J, Ruoff R S & H Lee, *Nat Commun*, 1 (2010) 1.
17 Pei S & Cheng H M, *Carbon*, 50 (2012) 3210.
18 Matsumoto M, Saito Y, Park C, Fukushima T & Aida T, *Nat Chem*, 7 (2015) 730.
19 Wang G, Yang J, Park J & Gou X, *J Phys Chem C*, 112 (2008) 8192.
20 Hummers W & Offeman R E, *J Am Chem Soc*, 80 (1958) 1339.
21 Saini P, Jalan R & Dhawan S K, *J Appl Polym Sci*, 108 (2008) 1437.